

Van der Waals interactions in the ground state of $\text{Mg}(\text{BH}_4)_2$ from density functional theory

A. Bil,¹ B. Kolb,² R. Atkinson,² D. G. Pettifor,¹ T. Thonhauser,^{2,*} and A. N. Kolmogorov^{1,†}

¹*Department of Materials, University of Oxford, Parks Road, Oxford OX1 3PH, United Kingdom*

²*Wake Forest University, Department of Physics, Winston-Salem, NC 27109 USA*

(Dated: April 20, 2022)

In order to resolve an outstanding discrepancy between experiment and theory regarding the ground-state structure of $\text{Mg}(\text{BH}_4)_2$, we examine the importance of long-range dispersive interactions on the compound's thermodynamic stability. Careful treatment of the correlation effects within a recently developed nonlocal van der Waals density functional (vdW-DF) leads to a good agreement with experiment, favoring the α - $\text{Mg}(\text{BH}_4)_2$ phase (P6₁22) and a closely related $\text{Mn}(\text{BH}_4)_2$ -prototype phase (P3₁12) over a large set of polymorphs at low temperatures. Our study demonstrates the need to go beyond (semi)local density functional approximations for a reliable description of crystalline high-valent metal borohydrides.

PACS numbers: 88.30.rd 63.20.-e 71.20.-b 78.30.-j

I. INTRODUCTION

Light-weight metal borohydrides remain in the spotlight of hydrogen-storage research due to their high gravimetric hydrogen content and abundance of the constituent elements.^{1,2} Li, Mg, and Ca tetraborohydrides ($M(\text{BH}_4)_n$) hold over 12 wt% of H, but their excessive thermodynamic stability presently renders these materials unsuitable for practical reversible hydrogen-storage solutions.¹ In an effort to adjust the formation enthalpies and the decomposition temperatures, several groups have suggested destabilization routes via reactions with other hydrides (see e.g. Refs.³⁻⁵) or synthesis of mixed metal tetraborohydrides (e.g. Li-Cu)⁶. Detailed knowledge of materials' ground states becomes essential, as the possibility of new compound formation depends on small free energy differences for the phases involved.

Metal tetraborohydrides are held together primarily by a combination of covalent (B-H) and ionic ($[M]^{n\delta+}$ - $[\text{BH}_4]^{n\delta-}$) interactions. Packing of the fairly rigid $[\text{BH}_4]^{n\delta-}$ units and $[M]^{n\delta+}$ ions into crystalline structures depends strongly on the valency and size of the metal atom, with exceptionally complex configurations occurring for the medium-sized divalent magnesium. Based on the experimental data, the ground states below and above $T = 453$ K, namely α and β , have been assigned space groups P6₁22 (330 atoms/u.c.)^{7,8} and Fddd (704 atoms/u.c.)⁹, respectively. Strikingly, numerous density functional theory (DFT) studies^{7,10-15} have converged on a completely unrelated F222 structure as the most stable low- T polymorph.^{12,14,15} Recently, it has been pointed out¹⁶ that the lack of a proper description of dispersion forces in the standard DFT approach may be a factor favoring low-density F222 structure over the experimental α phase.

In this study we take a key step towards resolving the existing discrepancy: we demonstrate that the weak dispersive interactions, important in other ionic (KCl and KBr)¹⁷ and covalent-ionic ($\text{Mg}(\text{OH})_2$ and $\text{Ca}(\text{OH})_2$)¹⁸

systems, indeed play a critical role in defining the $\text{Mg}(\text{BH}_4)_2$ ground state. We show that the commonly used Ceperley-Alder¹⁹ or Perdew, Burke, and Ernzerhof (PBE)²⁰ functionals artificially stabilize configurations with unusually high and low density, respectively. Inclusion of the dispersive contributions via a nonlocal van der Waals density functional (vdW-DF)^{21,22} or as a semi-empirical PBE-D* correction²³⁻²⁵ changes the relative stability of considered structures and favors the layered motif²⁶ occurring in related α - $\text{Mg}(\text{BH}_4)_2$ and $\text{Mn}(\text{BH}_4)_2$ prototypes.

The careful re-examination of $\text{Mg}(\text{BH}_4)_2$ has become possible due to a recent surge of attempts to include vdW interactions in the DFT.^{27,28} The truly nonlocal correlation functional in the vdW-DF approach has shown good transferability for a range of systems reaching from simple dimers²⁹ and physisorbed molecules³⁰ to DNA³¹ and drug design³². An efficient FFT formulation of vdW-DF³³ has allowed us to calculate the $T = 0$ K relative stability for $\text{Mg}(\text{BH}_4)_2$ structures of unprecedented size (up to 330 atom/u.c.). Calculation of the Gibbs energy vibrational contributions at finite temperatures is much more computationally demanding. In order to examine the relative stability as a function of temperature we have employed a semi-empirical method developed by Grimme^{24,25}, that includes the long-range contributions via damped pairwise $f_{\text{dmp}}(R)C_6R^{-6}$ terms at a negligible cost compared to standard DFT calculations. The method has gained popularity providing an improved description of molecular systems. However, Civalleri *et al.*^{18,23} demonstrated the need to adjust the parameterization (from PBE-D to PBE-D*) for the application of the method to crystalline solids and we observe a better transferrability of the modified set for the challenging case of $\text{Mg}(\text{BH}_4)_2$.

We describe the considered library of structure types and the simulation settings in Sec. II, present our systematic comparison of the performance of five DFT-based methods for $\text{Mg}(\text{BH}_4)_2$ at $T = 0$ K in Sec. III, demonstrate the effect of vibrational entropy on the poly-

morphs' relative stability at finite temperatures in Sec. IV, and conclude in Sec. V.

II. SIMULATION SETUP

Library of structure types. In addition to a large pool of previously considered candidate structures, we include potentially relevant $A(BC_4)_2$ prototypes found in the Inorganic Crystal Structure Database (ICSD)³⁴; the full list of 36 structures is given in Table I. All energies are referenced to the experimental low- T α phase, which has been recently argued to have a higher symmetry ($P6_122$)^{7,8} than originally thought ($P6_1$)^{9,35}. Our simulations confirm that, while the two structures are nearly degenerate in energy, only $P6_122$ is dynamically stable ($P6_1$ has multiple imaginary phonon modes reaching $50i$ cm^{-1}). The structure of the high- T β -phase, observed experimentally to be stable between 453 K and 613 K^{9,35}, remains an open question: the first powder diffraction orthorhombic solution with the $Fddd$ symmetry, based on the positions of the B and Mg atoms, has six imaginary phonon modes at Γ reaching $65i$ cm^{-1} . Notable $\text{Mg}(\text{BH}_4)_2$ candidates identified in previous DFT studies include the trigonal $P\bar{3}m1$ structures¹⁰ as well as the unusual low-density $F222$ phase derived from $I\bar{4}m2$ ^{12,14}. Figures 1a–c illustrate the diversity of the morphologies as different arrangements of the $\text{Mg}^{2\delta+}$ ions and $\text{BH}_4^{\delta-}$ units result in layered, hollow-framework-like, or fairly uniform densely-packed structures.

Simulation settings. The total energy calculations are carried out in the generalized gradient approximation (GGA) with the PBE²⁰ exchange-correlation (xc) functional and the local density functional approximation (LDA)¹⁹ as implemented in VASP³⁶. We employ projector augmented-wave pseudopotentials (PAW)³⁷ in which the semicore states are treated as valence. An energy cutoff of 500 eV and dense Monkhorst-Pack \mathbf{k} -point meshes ($\sim 0.03\text{\AA}^{-1}$ in each direction in the Brillouin zone)³⁸ are applied. The vdW-DF, PBE, PBE-D, and PBE-D* calculations are performed with a modified version of PWscf³⁹ using ultrasoft pseudopotentials. All structures were fully relaxed with the threshold of 10^{-5} [Ry] for energy convergence and $3 \cdot 10^{-1}$ [Ry a.u.⁻¹] for residual force; the residual stress was typically under 1 kbar. Benchmark tests given in Appendix A suggest that for a given xc functional the errors arising from other factors (convergence criteria, choice of pseudopotential, ect.) are rather small allowing us to resolve polymorphs ~ 0.005 eV/ BH_4 apart. Phonon spectra and the Gibbs energy corrections for selected structures are calculated with PBE and PBE-D* with a finite displacement method as implemented in PHON⁴⁰. Forces for phonon calculations were obtained from VASP (PBE) or QMPOT^{41,42} linked to VASP (PBE-D*) (for more details see Sec. IV).

Semiempirical dispersion contributions. The Grimme

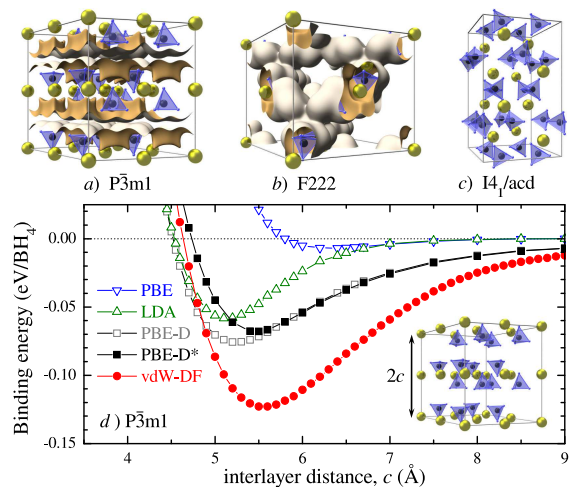


FIG. 1: (Color online) *a–c*) Hypothetical structures of $\text{Mg}(\text{BH}_4)_2$ with magnesium, boron, and hydrogen atoms shown as large (yellow), medium (black), and small (blue) spheres. The isosurfaces corresponding to charge density of $0.06 \text{ e}\text{\AA}^{-3}$ illustrate the layered and the 3D hollow framework structure of $P\bar{3}m1$ and $F222$ phases, respectively; anisotropy of the charge density in $I4_1/acd$ (not shown) is less pronounced. *d*) Binding energy as a function of the interlayer spacing in $P\bar{3}m1$ - $\text{Mg}(\text{BH}_4)_2$; the layers are allowed to relax but the intralayer distortions are insignificant.

corrections^{24,25} are introduced as

$$E_{\text{disp}} = -s_6 \sum_{i=1}^{N_{\text{at}}-1} \sum_{j=i+1}^{N_{\text{at}}} \frac{C_6^{ij}}{R_{ij}^6} f_{\text{dmp}}(R_{ij}), \quad (1)$$

where $C_6^{ij} = \sqrt{C_6^i C_6^j}$, $f_{\text{dmp}} = (1 + e^{-d(R_{ij}/R_r - 1)})^{-1}$, and R_r is the sum of individual R_0 .

For PBE-D calculations²⁵ we used the following set of C_6 coefficients [$\text{Jnm}^6 \text{mol}^{-1}$] and van der Waals radii R_0 [\AA]: for H atom $C_6 = 0.14$, $R_0 = 1.001$; for B atom $C_6 = 3.13$, $R_0 = 1.485$; for Mg atom $C_6 = 5.71$, $R_0 = 1.364$. Dimensionless parameter in the damping function and global scaling parameter are $d = 20$ and $s_6 = 0.75$, respectively. For PBE-D* parameterization²³ R_0 was multiplied by 1.3 (H), or by 1.05 factor (B, Mg).

III. PERFORMANCE OF DFT-BASED METHODS FOR $\text{Mg}(\text{BH}_4)_2$

The necessity to treat $\text{Mg}(\text{BH}_4)_2$ beyond the standard DFT approximations becomes evident when the PBE functional shows virtually no interlayer binding for the exemplary layered $P\bar{3}m1$ phase (Fig. 1d). The lack of a noticeable covalent or electrostatic interaction between the layers is a result of the particular packing of the BH_4 tetrahedra that makes the interlayer interface consist of two parallel sheets of hydrogen atoms already engaged in covalent B-H bonds. Introduction of

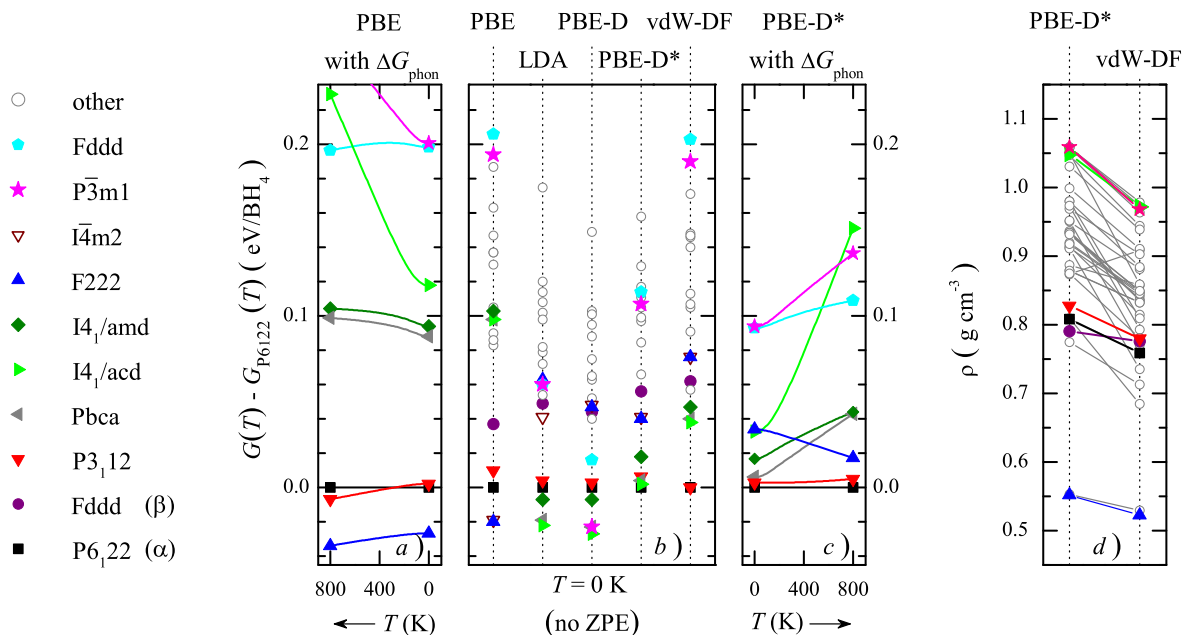


FIG. 2: (Color online) *a-c*) Relative Gibbs energy of selected Mg(BH₄)₂ polymorphs referenced to the P6₁22 phase: in *b*) the relative energy is shown for all five approximations at $T=0$ K without zero point energy while in *a,c*) vibrational contributions to $G(T)$ are included for PBE and PBE-D*. *d*) Density of Mg(BH₄)₂ polymorphs fully relaxed with PBE-D* and vdW-DF methods ($\rho_{\alpha}^{\text{exp}} = 0.782$ g cm⁻³)⁸.

the vdW interactions via vdW-DF, PBE-D, and PBE-D* leads to interlayer cohesions of 0.123, 0.076, and 0.068 eV/BH₄, respectively. The size of the extra binding is substantial considering that the reported energy difference between the experimental (α) and theoretical (F222) ground states within PBE is only 0.024 eV/BH₄¹⁵. The LDA, known to mimic dispersive interactions (e.g., in graphite⁴³), also gives a 0.058 eV/BH₄ binding, but – as we show below – should not be used as a substitute for a properly constructed nonlocal functional.

We compare the performance of the five different methods, PBE, LDA, PBE-D, PBE-D*, and vdW-DF, by plotting the relative stability and compound density for selected structures in Fig. 2 (the corresponding values for all 36 structures are listed in Table I). A number of unexpected features emerge as we examine the total energy data moving from left to right in Fig. 2b. At the PBE level, we find the highest stability of the least compact F222 phase, in agreement with Ref.¹³. However, in the LDA, arguably better suited for simulating Mg(BH₄)₂ based on our test in Fig. 1, there is a dramatic change in the ordering of the polymorphs' enthalpies with the ground state now being the most compact I4₁/acd structure. It is evident that, compared to PBE, the LDA favors higher packing: it lowers the relative enthalpy of the two densest P $\bar{3}m1$ and I4₁/acd polymorphs by 0.134 and 0.120 eV/BH₄, respectively, and increases the relative enthalpy of the sparsest F222 by 0.083 eV/BH₄.

Inclusion of the dispersive contribution in PBE-D also

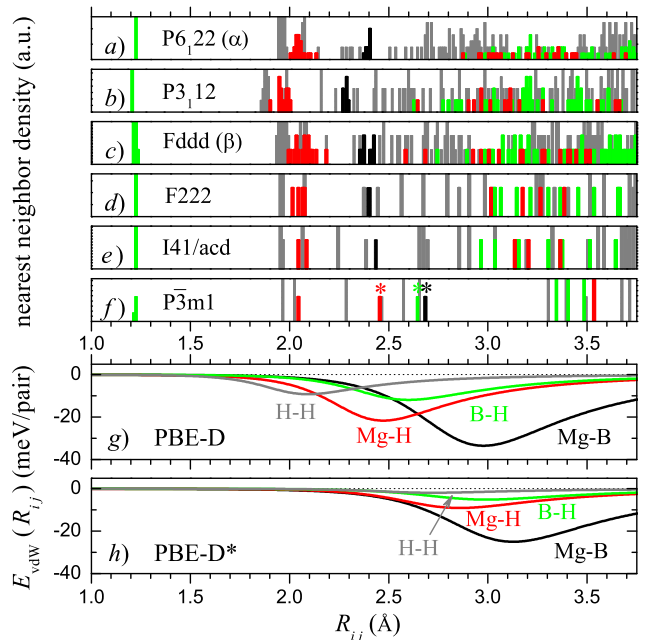


FIG. 3: (Color online) *a - f*) Nearest neighbor histograms in selected structures fully relaxed in PBE-D*; the stars in *f*) mark intralayer distances. *g, h*) Strength of pairwise Grimme corrections in the PBE-D and PBE-D* parameterizations.

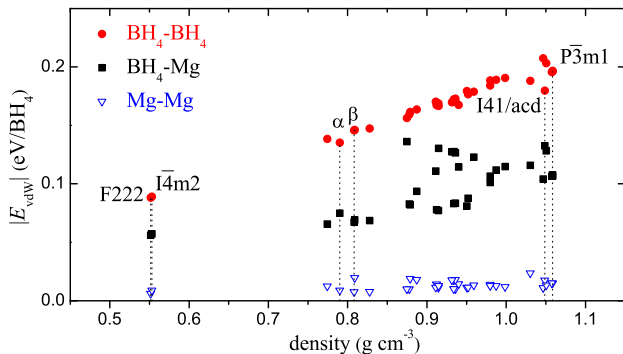


FIG. 4: (Color online) Breakdown of dispersion energy contributions calculated at PBE-D* level as a function of polymorph density for $\text{Mg}(\text{BH}_4)_2$ structures listed in Table I.

leads to a significant reordering of the relative stabilities obtained with PBE and promotes the $\text{I4}_1/\text{acd}$ structure. In fact, there is more agreement between the LDA vs PBE-D rather than the PBE vs PBE-D sets. The $\text{P}\bar{3}\text{m1}$ polymorph gets an even larger 0.217 eV/ BH_4 gain in relative stability dropping below α by 0.023 eV/ BH_4 , which may look surprising given the similar size of the interlayer binding for this structure in LDA and PBE-D (Fig. 1). To help explain this result we plot pairwise interaction strengths (Fig. 3g) and histograms of nearest neighbors (NNs) for relevant structures (Fig. 3a-f). It has been discussed^{23,27} that introduction of the dispersive interactions ‘on top’ of DFT requires a smooth cut-off of the attractive C_{ij}/R_{ij}^{-6} terms just below the typical vdW distances to avoid their unphysical contributions at short R_{ij} . Panels *f* and *g* in Fig. 3 show that a number of intralayer distances in $\text{P}\bar{3}\text{m1}$ (marked with stars) happen to fall in the critical range, around the corresponding $R_i^{\text{vdW}} + R_j^{\text{vdW}}$ values fitted to molecular datasets, which can give rise to artificially strong binding.

The suggested adjustment of the vdW parameters within PBE-D*²³ helps reduce the vdW overbinding for the dense $\text{P}\bar{3}\text{m1}$ and $\text{I4}_1/\text{acd}$ structures and for the first time we observe the α -phase to be the most stable polymorph among the considered diverse set of candidates, albeit by a small margin. The classical pairwise representation of the vdW corrections in the Grimme approach (Eq. 1) makes it possible to examine the individual vdW contributions. According to Fig. 3h, the increase in R_i^{vdW} values (from 1.001, 1.485, 1.364 Å to 1.301, 1.559, 1.432 Å for $i = \text{H}, \text{B}, \text{Mg}$, respectively) greatly diminishes the direct H-H interaction. However, Fig. 4 shows that the $\text{BH}_4\text{-BH}_4$ interaction still dominates the long-range binding, which – not unexpectedly – scales almost linearly with the crystal density. The second largest contribution, Mg-BH_4 , deviates from linear dependence due to a variable coordination of Mg ions. The classical attractive terms cause up to $\sim 20\%$ volume reduction compared to structures optimized with PBE.

Finally, the vdW-DF method correctly predicts α to be the low- T ground state and separates it from all other unrelated structures by a considerable 0.040 eV/ BH_4 ; the near degeneracy of α and P3_112 ($\text{Mn}(\text{BH}_4)_2$ prototype) can be traced to the close structural relationship between the two layered structures discussed in detail in Ref.²⁶. The method places the hypothetical F222 structure 0.076 eV/ BH_4 above α and differentiates between the two high-density 2D $\text{P}\bar{3}\text{m1}$ and 3D $\text{I4}_1/\text{acd}$ structures by improving the stability of just the latter. This suggests that the overestimation of the intralayer binding in the difficult $\text{P}\bar{3}\text{m1}$ case might still not be fully corrected within PBE-D*. Comparison of crystal densities for PBE-D* and vdW-DF in Fig. 2d shows that the latter results in less compact structures; the effect of the nonlocal correlations on the volume change is not easy to quantify because the method is based on the exchange and correlation functionals taken from revPBE⁴⁴ and LDA, respectively. The calculated vdW-DF value of $\rho = 0.758 \text{ g cm}^{-3}$ for the α phase is 3% below the experimental value which is consistent with a typical 1% overestimation of bond lengths for GGA-based methods.

IV. INCLUSION OF THE VIBRATIONAL CONTRIBUTIONS TO $G(T)$

Inclusion of finite temperature contributions due to the vibrational entropy is orders of magnitude more expensive than the calculation of the total energy at zero temperature. We estimate the vibrational corrections using two DFT-based methods, PBE-D and PBE-D*, which is computationally feasible and allows us to show directly the effect of the vdW interactions. Hessian matrices were calculated in a numerical fashion from analytical forces and atomic displacements for sufficiently large supercells (at least 88 atoms).⁴⁵ According to our extensive tests for $\text{Mg}(\text{BH}_4)_2$, the 0.00133 Å displacements and the 10^{-8} eV SCF energy convergence criterion ensured minimal errors ($\sim 10 \text{ cm}^{-1}$) for the calculated frequencies coming from the unharmonic effects and numerical factors. q -mesh for the dynamical matrices was typically two times denser than the k -mesh for the energy calculations in each direction. The analytical forces at the PBE level were found with VASP for fully relaxed polymorph structures. The analytical forces at the PBE-D* level were calculated using QMPOT linked with VASP. In this case, since QMPOT does not currently offer stress calculations, the structures were optimized as follows: the unit cells were first fully relaxed with PWscf and then the ionic positions were re-optimized with a combination of QMPOT and VASP. As described in Appendix A, our careful tests for selected structures showed insignificant variation in the equilibrium cell parameters in the two settings. Once the phonon densities of states $n(\omega)$ were found, the vibrational contributions $G_{\text{phon}}(T)$ were included via⁴⁰

$$G_{\text{phon}}(T) = k_{\text{B}}T \int_0^\infty \ln [2 \sinh(\hbar\omega/(2k_{\text{B}}T))] n(\omega) d\omega \quad (2)$$

Nr	Parent str.	Symm.	Z	vdW-DF		PBE-D*		PBE-D		PBE		LDA	
				ρ	ΔE	ρ	ΔE	ρ	ΔE	ρ	ΔE	ρ	ΔE
36	Mg(AlH ₄) ₂	P $\bar{3}m1$ (164)	1	0.780	0.439	0.875	0.550	0.948	0.543	0.735	0.606	0.975	0.684
35	Mg(BH ₄) ₂	P2/m (10)	2	0.793	0.405	0.915	0.447	1.061	0.345	0.807	0.517	1.112	0.433
34	Mg(BH ₄) ₂	P $\bar{3}$ (147)	9	0.845	0.341	0.936	0.322	0.985	0.241	0.848	0.409	1.037	0.350
33	Zn(ReO ₄) ₂	P $\bar{3}$ (147)	1	0.850	0.340	0.932	0.319	0.981	0.238	0.850	0.410	1.040	0.350
32	ZrMo ₂ O ₈	P $\bar{3}1c$ (163)	6	0.848	0.340	0.934	0.319	0.979	0.238	0.850	0.409	1.028	0.350
31	Mn(BF ₄) ₂	Pnma (62)	4	0.847	0.278	0.940	0.251	0.993	0.175	0.852	0.318	1.046	0.258
30	Mg(BH ₄) ₂	Pnmm (58)	2	0.735	0.266	0.911	0.270	0.980	0.250	0.775	0.320	1.015	0.297
29	Cr(AlCl ₄) ₂	Pca2 ₁ (29)	4	0.809	0.248	0.980	0.193	1.051	0.148	0.787	0.090	1.085	0.189
28	Mg(BH ₄) ₂	P2 ₁ /c (14)	2	0.872	0.245	0.959	0.173	1.011	0.092	0.816	0.186	1.052	0.174
27	Mg(BH ₄) ₂	P2 ₁ (4)	2	0.859	0.212	1.050	0.167	1.117	0.091	0.846	0.210	1.149	0.157
26	Ca(BH ₄) ₂	Fddd (70)	8	0.903	0.203	0.987	0.114	1.043	0.016	0.943	0.206	1.090	0.093
25	Mg(BH ₄) ₂	P2/m (10)	2	0.963	0.195	1.058	0.106	1.101	-0.023	0.946	0.193	1.157	0.060
24	Sr(AlCl ₄) ₂	P2/c (13)	2	0.978	0.194	1.058	0.107	1.101	-0.023	0.947	0.194	1.158	0.060
23	Mg(BH ₄) ₂	P $\bar{3}1m$ (162)	6	0.974	0.194	1.058	0.107	1.101	-0.023	0.947	0.194	1.153	0.060
22	Mg(BH ₄) ₂	P $\bar{3}m1$ (164)	1	0.968	0.191	1.058	0.107	1.101	-0.023	0.950	0.194	1.145	0.060
21	ZrMo ₂ O ₈	Pmn2 ₁ (31)	2	0.910	0.182	0.999	0.138	1.051	0.080	0.894	0.224	1.076	0.143
20	Be(BH ₄) ₂	I4 ₁ cd (110)	16	0.909	0.173	0.878	0.110	0.911	0.087	0.677	0.026	0.961	0.093
19	Mg(BH ₄) ₂	P $\bar{1}$ (2)	4	0.685	0.172	0.809	0.158	0.896	0.149	0.651	0.147	0.924	0.175
18	Mg(BH ₄) ₂	P1 (1)	2	0.780	0.149	0.915	0.111	0.964	0.040	0.760	0.086	0.986	0.098
17	Ba(BF ₄) ₂	P2 ₁ /c (14)	8	0.884	0.147	0.980	0.117	1.020	0.065	0.874	0.187	1.076	0.108
16	Be(AlO ₄) ₂	P $\bar{1}$ (2)	2	0.770	0.147	0.952	0.129	0.984	0.103	0.823	0.163	1.031	0.082
15	Mg(BH ₄) ₂	P2/c (13)	4	0.857	0.140	0.887	0.113	0.936	0.101	0.755	0.137	0.985	0.120
14	Mg(BH ₄) ₂	C2/c (15)	4	0.832	0.113	0.879	0.105	0.923	0.095	0.757	0.130	0.970	0.114
13	Mg(BH ₄) ₂	Pm (6)	1	0.877	0.107	0.950	0.099	0.978	0.075	0.841	0.137	1.017	0.079
12	Pt(SO ₄) ₂	P2 ₁ /c (14)	4	0.713	0.106	0.774	0.097	0.803	0.088	0.679	0.083	0.844	0.102
11	Ca(BF ₄) ₂	Pbca (61)	8	0.841	0.091	0.912	0.085	0.958	0.063	0.766	0.105	1.008	0.072
10	Mg(BH ₄) ₂	I $\bar{4}m2$ (119)	4	0.529	0.077	0.553	0.041	0.553	0.048	0.533	-0.019	0.585	0.041
9	Mg(BH ₄) ₂	F222 (22)	8	0.522	0.076	0.552	0.040	0.552	0.047	0.532	-0.020	0.591	0.063
8	Cd(AlCl ₄) ₂	Pc (7)	2	0.836	0.062	0.936	0.066	0.967	0.052	0.801	0.092	0.998	0.054
β	Mg(BH ₄) ₂	Fddd (70)	64	0.775	0.062	0.790	0.056	0.819	0.044	0.727	0.037	0.865	0.049
6	Mg(BH ₄) ₂	Pmc2 ₁ (26)	2	0.835	0.058	0.934	0.066	0.966	0.052	0.790	0.090	1.002	0.054
5	Mg(BH ₄) ₂	I4 ₁ /amd (141)	8	0.939	0.047	1.030	0.018	1.044	-0.007	0.974	0.103	1.082	-0.007
4	Sr(AlCl ₄) ₂	I4 ₁ /acd (142)	4	0.972	0.043	1.049	0.002	1.078	-0.027	0.986	0.098	1.102	-0.022
3	Sr(AlCl ₄) ₂	Pbca (61)	8	0.944	0.040	1.047	0.004	1.074	-0.023	0.979	0.098	1.100	-0.019
2	Mn(BH ₄) ₂	P3 ₁ 12 (151)	9	0.780	0.000	0.828	0.007	0.837	0.003	0.791	0.010	0.878	0.004
α	Mg(BH ₄) ₂	P6 ₁ 22 (178)	30	0.758	0	0.808	0	0.814	0	0.770	0	0.860	0

TABLE I: Relative stability ΔE [eV/BH₄] and density ρ [g cm⁻³] ($T = 0$ K, no zero point energy corrections) of magnesium borohydride polymorphs referenced to the experimentally observed α phase. Z stands for the number of Mg(BH₄)₂ formulas per unit cell. In the third column space groups information (international symbols and numbers) is reported.

Calculated relative Gibbs energies $G(T)$ for selected low-energy structures are shown in Fig. 2a and 2c. We find that the zero point energy alone can change the relative stability by over 0.04 eV/BH₄. Addition of dispersive interactions leads to about 0.01 eV/BH₄ changes in the relative stability at $T = 800$ K and can affect

the ordering of the polymorphs as happens for the P3₁12 structure. The related α and P3₁12 phases remain nearly degenerate in the whole T range and cannot be unambiguously resolved within our vdW-DF or PBE-D* simulations. The search for the high- T ground state may be simplified by our observation of little variation in the en-

enthalpy difference between α and β for all the five methods in Fig. 2: due to the close structural relationship between the two phases, shown in Fig. 3a and 3c, there must be a cancellation of errors. Hence, despite the remaining noticeable difference between the PBE-D* and vdW-DF relative stability for some polymorphs the former could be an appropriate choice for identification of viable high- T candidates and estimation of the phonon contributions to $G(T)$.

V. CONCLUSIONS

The presented results illustrate that identification of ground states depends not only on the exhaustive sampling of possible structures and compositions but also on the accuracy of the chosen simulation method. We have demonstrated that inclusion of the dispersive interactions via nonlocal correlation functional within vdW-DF leads to a good agreement with experiment for the $\text{Mg}(\text{BH}_4)_2$ low- T ground state. The related well-characterized $\text{Ca}(\text{BH}_4)_2$ system should be an interesting test case for the vdW-DF and PBE-D* methods since standard DFT approximations seem to already reproduce the experiment⁴⁶. Proper treatment of the nonlocal correlation effects is expected to be most critical in higher-valent metal borohydrides that can form weakly interacting molecular-type complexes¹⁶. Until such large crystalline systems can be handled with accurate quantum Monte Carlo-level or quantum chemistry methods, the continued improvement of DFT-based methods⁴⁷ may provide an attractive alternative for description of the dispersive interactions therein. In any case, it appears to be good practice to systematically test proposed ground states with a range of DFT flavours as this can help spot and avoid potential artifacts of DFT approximations.

VI. ACKNOWLEDGMENTS

A.B. and A.N.K. acknowledge the support of the EPSRC through the DTI Technology Program EP/D062098/1 and the CAF EP/G004072/1. Calculations were performed in the Gdansk Supercomputing Center, on the DEAC cluster of Wake Forest University, and in the Oxford Supercomputing Centre. A.B. thanks Bernhard Seiser for helpful discussions.

Appendix A: Benchmark tests

To estimate how technical factors, such as a choice of a pseudopotential, may influence the accuracy of total enthalpy calculations we performed an optimization of a set of exemplary structures at the PBE-D* level using the projector augmented-wave pseudopotentials (PAW)³⁷, as implemented in VASP, as well as the ultrasoft pseudopotentials (USPP)⁴⁸, as implemented in PWscf (see Table II). In the first case, we used QMPOT software linked to VASP to calculate dispersion contributions to energy and forces. A crystal cell has been optimized in a series of independent runs for a set of cell parameters. For all exemplary structures the relative difference in cell parameters optimized using PAW pseudopotential (VASP+QMPOT) and USPP pseudopotential (PWscf software) was below 0.5%. The difference between relative energies calculated with PAW and USPP was found to be below 0.0035 eV/ BH_4 . We estimate that for a given xc functional the errors arising from other factors (convergence criteria, choice of pseudopotential, ect.) are rather small allowing us to resolve polymorphs ~ 0.005 eV/ BH_4 apart.

	α	2	3	4	5	6	8	10	11	12	22
PAW	0.0000	0.0065	0.0029	0.0022	0.0188	0.0670	0.0671	0.0373	0.0848	0.0965	0.1091
USPP	0.0000	0.0065	0.0041	0.0022	0.0179	0.0660	0.0658	0.0406	0.0845	0.0968	0.1066
difference	0.0000	0.0000	-0.0012	0.0000	0.0009	0.0010	0.0013	-0.0033	0.0003	0.0003	0.0025

TABLE II: Relative enthalpy [eV/ BH_4] of selected polymorphs calculated at the PBE-D* level with different pseudopotentials.

* E-mail: thonhauser@wfu.edu

† E-mail: aleksey.kolmogorov@materials.ox.ac.uk

¹ T.K. Mandal and D.H. Gregory, *Annu. Rep. Prog. Chem., Sect. A* **105**, 21 (2009).

² L. Schlappbach and A. Züttel, *Nature* **414**, 353 (2001); W. Grochala and P.P. Edwards, *Chem. Rev.* **104**, 1283 (2004); S. Orimo, Y. Nakamori, J.R. Eliseo, A. Züttel, and C.M. Jensen *Chem. Rev.* **107**, 4111 (2007).

- ³ J.J. Vajo, S.L. Skeith, and F. Meters, *J. Phys. Chem. B* **109**, 3719 (2005).
- ⁴ S.V. Alapati, J.K. Johnson, and D.S.Sholl, *Phys. Chem. Chem. Phys.* **9**, 1438 (2007).
- ⁵ S.V. Alapati, J.K. Johnson, and D.S.Sholl, *J. Phys. Chem. C* **112**, 5258 (2008).
- ⁶ K. Miwa, N. Ohba, S. Towata, Y. Nakamori, and S.-I.Orimo, *J. Alloys Compd.* **404-406**, 140 (2005).
- ⁷ B. Dai, D. S. Sholl, and J. K. Johnson, *J. Phys. Chem. C* **112**, 4391 (2008).
- ⁸ Y. Filinchuk, R. Černý, and H. Hagemann, *Chem. Matter.* **21**, 925 (2009).
- ⁹ J-H. Her *et al.*, *Acta Cryst.* **B63**, 561 (2007).
- ¹⁰ Y. Nakamori *et al.*, *Phys. Rev. B* **74**, 045126 (2006).
- ¹¹ P. Vajeeston, P. Ravindran, A. Kjekshus, and H. Fjellvåg, *Appl. Phys. Lett.* **89**, 071906 (2006).
- ¹² V. Ozolins, E. H. Majzoub, and C. Wolverton, *Phys. Rev. Lett.* **100**, 135501 (2008).
- ¹³ J. Voss, J. S. Hummelshøj, Z. Lodziana, and T. Veege, *J. Phys.: Condens. Matter* **21**, 012203 (2009).
- ¹⁴ X.-F. Zhou *et al.*, *Phys. Rev. B* **79**, 212102 (2009).
- ¹⁵ R. Caputo, A. Tekin, W. Sikora, A. Züttel, *Chem. Phys. Lett.* **480**, 203 (2009).
- ¹⁶ Z. Lodziana, M. J. van Setten, *Phys. Rev. B* **81**, 24117 (2010); Z. Lodziana, *Phys. Rev. B* **81** 144108 (2010).
- ¹⁷ K. Doll and H. Stoll, *Phys. Rev. B* **56**, 10121 (1997).
- ¹⁸ P. Uglieno *et al.*, *J. Mater. Chem.* **19**, 2564 (2009).
- ¹⁹ D.M. Ceperley and B.J. Alder, *Phys. Rev. Lett.* **45**, 566 (1980); J.P. Perdew and A. Zunger, *Phys. Rev. B* **23**, 5048 (1981);
- ²⁰ J.P. Perdew, K. Burke, and M. Ernzerhof, *Phys. Rev. Lett.* **77**, 3865 (1996).
- ²¹ M. Dion *et al.*, *Phys. Rev. Lett.* **92**, 246401 (2004); **95**, 109902(E) (2005).
- ²² T. Thonhauser *et al.*, *Phys. Rev. B* **76**, 125112 (2007).
- ²³ B. Civalleri, C. M. Zicovich-Wilson, L. Valenzano, and P. Uglieno, *Cryst. Eng. Comm.* **10**, 405 (2008).
- ²⁴ S. Grimme, *J. Comput. Chem.* **25**, 1463 (2004).
- ²⁵ S. Grimme, *J. Comput. Chem.* **27**, 1788 (2006).
- ²⁶ R. Černý, N. Penin, H. Hagemann, and Y. Filinchuk, *J. Phys. Chem. C* **113**, 9003 (2009).
- ²⁷ S. Grimme, J. Anthony, T. Schwabe, and Ch. Mück-Lichtenfeld, *Org. Biomol. Chem.* **5**, 741 (2007).
- ²⁸ D. C. Langreth *et al.*, *J. Phys.: Condens. Matter* **21**, 084203 (2009).
- ²⁹ T. Thonhauser, A. Puzder, and D.C. Langreth, *J. Chem. Phys.* **124**, 164106 (2006); S. Li, V.R. Cooper, T. Thonhauser, A. Puzder, and D. C. Langreth, *J. Phys. Chem. A* **112**, 9031 (2008); J. Hooper, V. R. Cooper, T. Thonhauser, N. A. Romero, F. Zerilli, and D. C. Langreth, *ChemPhysChem* **9**, 891 (2008).
- ³⁰ M. Mura, A. Gulans, T. Thonhauser, and L. Kantorovich, *Phys. Chem. Chem. Phys.* **12**, 4759 (2010).
- ³¹ V. R. Cooper, T. Thonhauser, A. Puzder, E. Schröder, B. I. Lundqvist, and D. C. Langreth, *J. Am. Chem. Soc.* **130**, 1304 (2008); V. R. Cooper, T. Thonhauser, and D. C. Langreth, *J. Chem. Phys.* **128**, 204102 (2008).
- ³² S. Li, V. R. Cooper, T. Thonhauser, B. I. Lundqvist, and D. C. Langreth, *J. Phys. Chem. B* **113**, 11166 (2009).
- ³³ G. Román-Pérez and J. M. Soler, *Phys. Rev. Lett.* **103**, 096102 (2009).
- ³⁴ G. Bergerhoff and I.D. Brown, in *Crystallographic Databases*, edited by F.H. Allen *et al.* (International Union of Crystallography, Chester,1987).
- ³⁵ R. Černý, Y. Filinchuk, H. Hagemann, and K. Yvon, *Angew. Chem. Int. Ed.* **46**, 5765 (2007).
- ³⁶ G. Kresse and J. Hafner, *Phys. Rev. B* **47**, 558 (1993); G. Kresse and J. Furthmüller, *Phys. Rev. B* **54**, 11169 (1996).
- ³⁷ P. E. Blöchl, *Phys. Rev. B* **50**, 17953 (1994).
- ³⁸ J. D. Pack and H. J. Monkhorst, *Phys. Rev. B* **13**, 5188 (1976); **16**, 1748 (1977).
- ³⁹ P. Giannozzi *et al.*, *J. Phys. Condens. Matter* **21**, 395502 (2009).
- ⁴⁰ D. Alfè, *Comp. Phys. Commun.* **180**, 2622 (2009).
- ⁴¹ M. Sierka and J. Sauer, *J. Chem. Phys.* **112**, 6983 (2000).
- ⁴² T. Kerber, M. Sierka, and J. Sauer, *J. Comput. Chem.* **29**, 2090 (2008).
- ⁴³ A.N. Kolmogorov and V.H. Crespi, *Phys. Rev. B* **71**, 235415 (2005).
- ⁴⁴ Y. Zhang and W. Yang, *Phys. Rev. Lett.* **80**, 890 (1998).
- ⁴⁵ We used $1 \times 1 \times 1$ simulation cell for α , P3₁12, Pbc_a, Fddd and $2 \times 2 \times 2$ simulation supercell for I4₁/acd, I4₁/amd, F222, P $\bar{3}$ m1, respectively.
- ⁴⁶ Y.-S. Lee *et al.*, *Phys. Rev. B* **79**, 104107 (2009).
- ⁴⁷ A. Tkatchenko and M. Scheffler, *Phys. Rev. Lett.*, **102** 073005 (2009); J. Klimes, D.R. Bowler, and A. Michaelides, *J. Phys.: Condens. Matter* **22**, 022201 (2010).
- ⁴⁸ downloaded from <http://www.pwscf.org/>